Application of phase retrieval algorithm in reflective tomography laser radar imaging

Xiaofeng Jin (金晓峰)*, Jianfeng Sun (孙建锋), Yi Yan (严 毅), Yu Zhou (周 煜), and Liren Liu (刘立人)

Key Laboratory of Space Laser Communication and Testing Technology, Shanghai Institute of Optics and Fine Mechanics, Chinese Academy of Sciences, Shanghai 201800, China

**Corresponding author: jxf2008@siom.ac.cn*

Received June 9, 2010; accepted August 11, 2010; posted online January 1, 2011

We apply phase retrieval method to align projection data for tomographic reconstruction in reflective tomography laser radar imaging. In our experiment, the target is placed on a spin table with an unknown, but fixed, axis. The oscillatory motion of the target in the incident direction of the laser pulse is added at each view to simulate the real satellites random motion. The experimental simulation results demonstrate the effectiveness of this method to improve image reconstruction quality. Future research also includes the development of projection registration based on phase retrieval for targets with more complicated structure.

OCIS codes: 280.3640, 100.3020, 100.5070.
doi: 10.3788/COL201109.012801.

Reflective tomography is one of the most effective high-resolution imaging methods in laser radar imaging systems. The range-resolved laser reflective tomography imaging laser radar was first introduced by Parker *et al.*[1−4] Several years later, Matson *et al.* began exploring the technique of using the HI-CLASS coherent laser radar system to obtain reflective images by carrying out a heterodyne system analysis, deriving and validating imaging signal-to-noise ratio (SNR) expressions, and so on[5−11].

The range to the target in incoherent direct detection of range-resolved reflective tomography cannot be measured with sufficient accuracy to align the intensity projections to an appropriate center of rotation. This would bring serious artifacts in the final images reconstructed. However, displacement of the individual projection in the incident direction of laser pulse only produces linear phase errors in their Fourier transforms. In theory, the Fourier modulus of each projection is unaffected by the misalignments in the incident direction. We can infer the Fourier modulus of the target from the misaligned projections by using the Fourier slice theorem for tomographic reconstruction. The phase retrieval algorithm developed by Fienup[12,13] can be used for the object image recovery. Ford *et al.* first introduced this iterative technique to automatically align simulated projection data for reflective tomography[10]. However, in their presentation, the projections were required to satisfy the assumptions associated with transmission tomography by computer simulation. In other words, they simulately absorbed, rather than reflected, the signal. Afterwards, Matson *et al.* mentioned the phase retrieval algorithm[11]; however, the imaging results of the phase retrieval algorithm in reflective tomography has not been reported. In this letter, we present the first image reconstruction results of a target by using phase retrieval algorithm in the range-resolved reflective tomography techniques.

A brief review of mathematical foundations, including filtered back-projection and Radon-Fourier transform[1−3], is first provided for reflective tomograpic reconstruction. Let $f(x,y)$ denote the image to be reconstructed, and $L_{r,\phi}$ denote the solid line $r = x\cos\phi + y\sin\phi$ (Fig. 1(a))

$$p(r,\phi) = \int_{L_{r,\phi}} f(x,y)\mathrm{d}s, \tag{1}$$

where s represents the solid line along $L_{r,\phi}$, $p(r,\phi)$ is the projection of the target $f(x,y)$ at angle ϕ, and the variable r denotes the spatial variable along the integration path in the ϕ direction.

Using back-projection, the reconstructed image $g(x,y)$ is given by

$$g(x,y) = \sum_{i=1}^{m} F_1^{-1}\left\{\widetilde{c}F_1[p(r,\phi)]\right\}\Delta\phi, \tag{2}$$

where ϕ_i is the angle of the ith projection, $\Delta\phi$ is the sampling angular separation, m is the total number of projections, F_1 and F_1^{-1} denote the one-dimensional (1D) Fourier transform and the inverse Fourier transform operators; r represents space variable; $\widetilde{c}$ is the filter function, which is the product of a window function and the magnitude of the spatial frequency[1,2,5,6,16,17].

The Radon-Fourier transform method is based on Fourier slice theorem, which states that the 1D Fourier transform of a projection is a slice through the two-dimensional (2D) Fourier transform of the target. In mathematics, the Fourier slice theorem can be expressed as

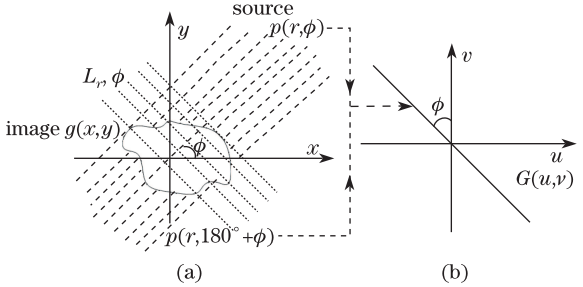

Fig. 1. Diagram of reflective tomography.

$$G(u\cos\phi, v\sin\phi) = P(K,\phi), \tag{3}$$

where $P(K,\phi) = F_1[p(r,\phi)]$, $G(u,v) = F_2[g(x,y)]$, F_2 denotes the 2D Fourier operator. By collecting projection data at a number of angles, recovering a complete estimate of Fourier transform without directly measuring all points in the target is possible. Then, the 2D image recovery can be generated by using an inverse Fourier transform. For conventional transmission tomography, the integrated transmission in the direction ϕ is equivalent to $180^\circ + \phi$. However, for reflective tomography, the projection $p(r,\phi)$ and $p(r, 180^\circ + \phi)$ leads to a different Fourier estimate along the same line $\phi + 90^\circ$ through the origin. Figures 1(a) and (b) show the process above. In this case, the average of the two estimates will be used[2].

Notably, for all angles, all the Fourier-transformed slices intersect at zero spatial frequency and should be approximately equal to one another at this point. The reflectivity of the target is a function of the incident angle and surface reflective characteristics; therefore, the zero-spatial frequency value of each projection can be quite different. Therefore, normalization coefficient α_φ should be introduced to enforce that all projections have the same values at zero spatial frequency[11]. The modified Fourier slice formula for reflective tomography can be given by

$$\frac{\alpha_\phi\{F_1[p(r,\phi)]\} + \alpha_{\phi+180^\circ}\{F_1[p(r,\phi+180^\circ)]\}}{2} = G(-u\sin\phi, v\cos\phi). \tag{4}$$

Using the modified reflective tomography Fourier slice theorem, the Fourier modulus estimates of the 2D image to be reconstructed can be obtained. The next problem is to find an object consistent with the measured Fourier modulus. Phase retrieval is introduced below.

Phase retrieval algorithm was first introduced by Gerchberg *et al.*[18] to recover a 1D wave function from Fourier data[19]. Subsequently, Fienup *et al.* modified the above algorithm to address the phase retrieval problem for the reconstruction of stellar interferometry data[12–15]. A general block diagram of these two iterative algorithms is available in Fig. 2.

The mathematic formula of error reduction is given by

$$g_{k+1}(x,y) = \begin{cases} g'_k(x,y) & (x,y) \notin \gamma \\ 0 & (x,y) \in \gamma \end{cases}; \tag{5}$$

the mathematic formula of hybrid input and output is given by

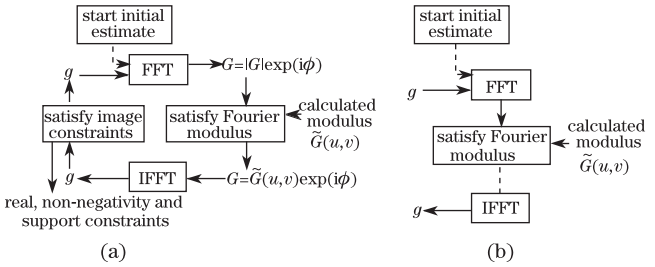

Fig. 2. (a) Error reduction algorithm; (b) hybrid input and output algorithm. FFT: fast Fourier transform; IFFT: inverse FFT.

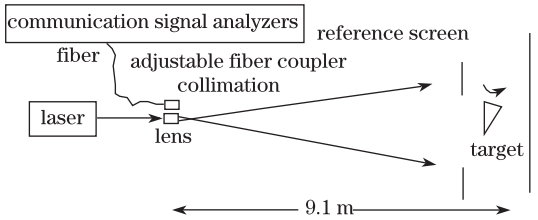

Fig. 3. Experimental setup used to measure range-resolved reflective tomography.

$$g_{k+1}(x,y) = \begin{cases} g'_k(x,y) & (x,y) \notin \gamma \\ g_k(x,y) - \beta g'_k(x,y) & (x,y) \in \gamma \end{cases}, \tag{6}$$

where γ includes all points at which $g'(x,y)$ violates the object constraints; β is a constant, $\beta = 0.7$ in this letter; and k is the iteration number.

The experimental setup used to measure range-resolved data is shown in Fig. 3. A triangular prism was illuminated by 8-ps, 1064-nm pulses with Gaussian profile from a passive Q-switched pulsed laser. Monostatic waveform was detected and recorded every 50 ps by a Tektronix series TDS7000B communication signal analyzer for a total time of 25 ns. The corresponding distance resolution of system was 7.5 mm because of the reflection off of the target. The distance between the detector and the target was set at 9.1 m because of the space constraint in the laboratory scale. The target was a triangular prism (30-cm axial height). The target was rotated around an unknown and fixed axis perpendicular to the direction of incident radiation. The projections were sampled at 1° steps from 0° to 360°.

Figure 4 shows the collected projection data and the corresponding views relative to the target. Then, the standard tomographic method of filtered back-projection was applied to the set of projections to produce a 2D image. The image reconstructed has the dimensions of range versus range, as if the target was being viewed along the rotation axis, as illustrated in Fig. 5.

In actual Doppler-time-intensity (DTI) detection, the relative motion of the target manifests itself as an oscillatory curve[21]. We suppose an approximate oscillatory motion of the target in the incident direction of laser pulse at range-resolved adjacent views[10]. First, a random amount of translation was simulated for each aligned projection. High-frequency components of the random displacements were not appropriate for translations because of the continuity of target motion. A second order inertial filter was assigned to adjust the random amounts to accord with real satellite vibrations. The final simulated displacements could be the combination of many low frequencies. The standard projections were translated by moving each projection away from the center of alignment by the filtered random amount (1–15 pixels), as shown in Fig. 6. The degraded image reconstructed by filtered back-projection with above misaligned projections is shown in Fig. 7.

The Fourier modulus estimates of the target can be obtained from the misaligned projection data using the Fourier slice theorem for reflective tomography. This reconstructed Fourier spectrum is on a polar grid. Polar to rectangular coordinate transformation is necessary for Fourier transform. Details are discussed in Refs. [22,23].

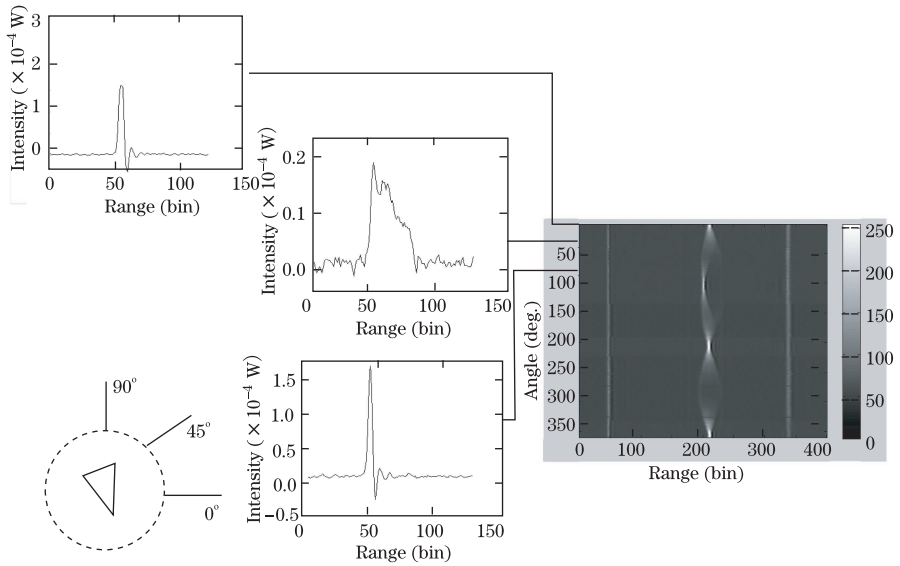

Fig. 4. Integrated diagram of projections viewed in 360° for reflective tomography. 1 bin=7.5 mm.

Fig. 5. Image reconstructed by filtered back-projection after threshold processing.

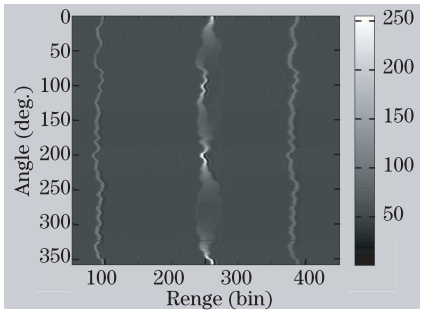

Fig. 6. Projections with misalignments.

The rectangular grid Fourier spectrum is then filtered with the $|k|$ filter to boost the high spatial frequencies and avoid artifacts. Figure 8(a) shows the Fourier modulus estimates $|\widetilde{G}(u,v)|$ from the misaligned projections. Figure 8(b) shows Fourier modulus $|G(u,v)|$ of the image reconstructed with aligned projections (Fig. 5). The mean square error (MSE) in the Fourier domain before phase retrieval can be given by

$$E_{\mathrm{F}} = \left[\frac{\sum_{u,v}[|\widetilde{G}(u,v)| - |G(u,v)|]^2}{\sum_{u,v}|G(u,v)|^2}\right]^{1/2} = 0.9924. \quad (7)$$

The diameter of the target can be computed from the Fourier modulus because it is half the diameter of the

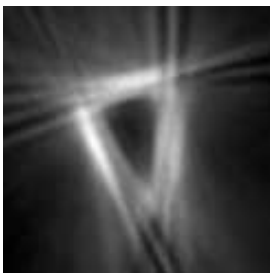

Fig. 7. Image reconstructed by projections with misalignments.

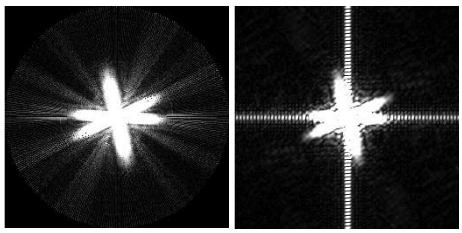

(a) (b)

Fig. 8. (a) Fourier modulus $|\widetilde{G}(u,v)|$ from the aligned projections using Fourier slice theory; (b) Fourier modulus $|G(u,v)|$of Fig. 5.

autocorrelation,

$$g(x,y) \star g(x,y) = F_2^{-1}\{|\widetilde{G}(u,v)|^2\}, \quad (8)$$

where $\star$ denotes autocorrelation operation, and F_2^{-1} denotes 2D inverse Fourier operator. Another object domain constraint is the need for $g(x,y)$ to be real and non-negative. The phase retrieval algorithm was combined with 20 iterations of error reduction method and 100 iterations of hybrid input-output method for faster convergence[14]. Three rectangular support masks with different initial guesses were used; the corresponding imaging results are shown in Fig. 9.

When the degraded image (Fig. 7) or constant matrix was used as the initial guess, we could obtain stable image recovery results. In Fig. 9(a), the degraded image is used and the MSE after phase retrieval is 0.4097; in

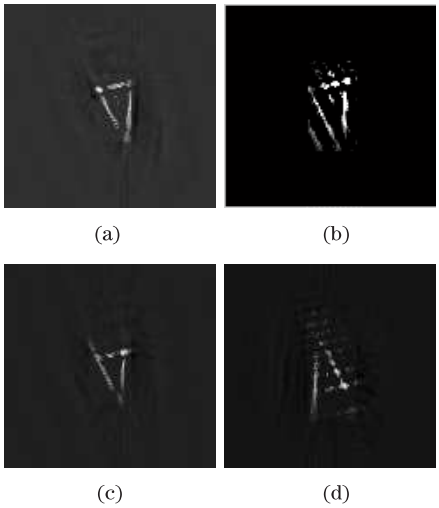

Fig. 9. Phase retrieval results using different initial guesses. (a) Degraded images as the initial guess, (b) constant matrix as the initial guess, (c) and (d) random matrix as the initial guess

Fig. 9(b), constant matrix is used and the MSE after phase retrieval is 0.3773. When random matrix is used as the initial guess, the MSE after phase retrieval is approximately 0.4506. The retrieval results are in an unstable state according to Figs. 9(c) and (d). The reduced-area support constraint method can be used to overcome these simultaneous twin images; details can be found in Ref. [15]. Finding that the constant matrix has better convergence than the others is easy when the value of MSE is used. For better reconstruction of these three initial guesses, the object support constraint should be changed in the process of phase retrieval algorithm. The first several iterations require to define a smaller support mask that tightly constrains the object; this helps to force most energy of the image into a confined region in less iteration. Afterwards, the support mask should be enlarged to the correct support constraints for the object. For the later iterations, a larger support constraint should be used to ensure that none of the target part is truncated by the constraint[14]. Finally, all the recovery images could be in stable state. Although there were artifacts in the reconstructed images, the general shape of the triangular prism was clearly recognized, and the size of the image reconstruction results matched approximately with the real target. We also collected data on another group of simulated misalignments for projections to validate the adaptability of this phase retrieval method, and the final image reconstruction was consistent with the former results.

In conclusion, we have demonstrated projection registration in range-resolved reflective tomography image reconstruction using a phase retrieval method to solve the issues of the unknown location of the axis of rotation and random target translation in the incident direction of laser pulse. Results show that limited distance of 9.1 m and range resolution of 7.5 mm in projections work well on experimental simulated misaligned projection data to improve the quality of image reconstruction. The combination of error reduction and hybrid input-output iteration developed by Fienup is used to improve algorithm convergence. Three support masks with different initial guesses are used. The general shape of the target is clearly recognized in the recovered images, and the size approximately matches that of the real target.

In the real world, the targets are always in complicated motions, and the simple motion model in this letter is just at the preliminary stage of research. In this experiment, a simple diffuse target is used. However, the realistic surface materials are the combination of diffuse and specular reflective characteristics[1,24]. This discrepancy between model and actual data may interfere with the convergence of the phase retrieval algorithm[10]. Robustness of this algorithm for different surfaces of the target will be investigated in the next project.

This work was supported by the National Natural Science Foundation of China under Grant No. 0803371-X00.

References

1. J. K. Parker, E. B. Craig, D. I. Klick, F. K. Knight, S. R. Kulkarni, R. M. Marino, J. R. Senning, and B. K. Tussey, Appl. Opt. **27,** 2642 (1988).
2. R. M. Marino, R. N. Capes, W. E. Keicher, S. R. Kulkarni, J. K. Parker, and L. W. Swezey, Proc. SPIE **999,** 248 (1988).
3. F. K. Knight, D. Klick, D. P. Ryan-Howard, J. R. Theriault, Jr., B. K. Tussey, and A. M. Beckman, Appl. Opt. **28,** 2196 (1989).
4. F. K. Knight, D. I. Klick, D. P. Ryan-Howard, and J. R. Theriault, Jr., Opt. Eng. **30,** 55 (1991).
5. C. L. Matson, E. P. Magee, and D. H. Stone, Proc. SPIE **2302,** 73 (1994).
6. E. P. Magee, C. L. Matson, and D. H. Stone, Proc. SPIE **2302,** 95 (1994).
7. C. L. Matson, Proc. SPIE **2562,** 184 (1995).
8. C. L. Matson, E. P. Magee, and D. E. Holland, Opt. Eng. **34,** 2811 (1995).
9. C. L. Matson, Opt. Commun. **137,** 343 (1997).
10. S. D. Ford and C. L. Matson, Proc. SPIE **3815,** 189 (1999).
11. C. L. Matson and D. E. Mosley, Appl. Opt. **40,** 2290 (2001).
12. J. R. Fienup, Opt. Lett. **3,** 27 (1978).
13. J. R. Fienup, Opt. Eng. **18,** 529 (1979).
14. J. R. Fienup, Appl. Opt. **21,** 2758 (1982).
15. J. R. Fienup and C. C. Wackerman, J. Opt. Soc. Am. A **3,** 1897 (1986).
16. D. Zhang and X. Dong, Acta Acustica (in Chinese) **20,** 271 (1995).
17. X. Jin, J. Sun, Y. Yan, Y. Zhou, and L. Liu, Acta Opt. Sin. (in Chinese) **30,** 747 (2010).
18. R. W. Gerchberg and W. O. Saxton, Optik **35,** 237 (1972).
19. Y. Liu, M. Zhang, X. Shen, Q. Wei, and S. Han, Acta Opt. Sin. (in Chinese) **27,** 2075 (2007).
20. J. Sun, X. Jin, and L. Liu, Proc. SPIE **7419,** 74190W (2009).
21. K. I. Schultz and S. Fisher, Appl. Opt. **31,** 7690 (1992).
22. H. Stark, J. Opt. Soc. Am. **69,** 1519 (1979).
23. H. Stark, J. W. Woods, I. Paul, and R. Hingorani, IEEE Trans. Acoustics, Speech and Signal Processing **29,** 237 (1981).
24. X. Jin and R. Y. Levine, Appl. Opt. **48,** 4191 (2009).